THE ASIAN BULLETIN OF BIG DATA MANAGMENT
Vol. 5. Issue 3 (2025)
https://doi.org/10.62019/abbdm.v5i3.372


# YOLO-v9-YOLO-v11: Brain Tumor Performance Analysis Using MRI Images

Anjum Ali, Moeez Bin Nadeem, Muhammad Waqas Aziz*, Muhammad Waleed Ashraf, Ghulam Mustafa

## Chronicle

**Article history**
**Received**: June 24, 2025
**Received in the revised format:** July 18, 2025
**Accepted:** Aug 8, 2025
**Available online:** Aug 26, 2025

**Anjum Ali, Moeez Bin Nadeem, Muhammad Waqas Aziz*, Muhammad Waleed Ashraf, & Ghulam Mustafa** are **currently** affiliated with the Riphah International University, Faisalabad, Pakistan.
**Email:** malik.anjumali@gmail.com
**Email**: moeez1280@gmail.com
**Email:** bismillahwaqas@gmail.com
**Email:** waleed_terhana@hotmail.com
**Email:** ghulammustafanfc@gmail.com

**Corresponding Author***

## Abstract

Early and accurate detection of brain tumors in Magnetic Resonance Imaging (MRI) scans is essential for effective treatment and improved patient survival. Although MRI is a widely used diagnostic tool, the manual interpretation of these images is often time-consuming and prone to variability among medical professionals. In biomedical imaging, deep learning methods have been increasingly explored to address these challenges, particularly for automated tumor detection and segmentation. This study compares three advanced object detection models—YOLO-v9, YOLO-v10, and YOLO-v11—evaluated on a dedicated brain tumor MRI dataset. Performance was assessed using multiple metrics, including precision, recall, F1-score, Intersection over Union (IoU), and mean Average Precision (mAP) at 0.5:0.95. In addition, Non-Maximum Suppression (NMS) and frames-per-second (FPS) rates were examined to determine efficiency and feasibility for real-time inference. The results demonstrate that all three YOLO-based architectures achieve high accuracy and efficiency, highlighting their suitability for medical image analysis. Among them, YOLO-v10 achieved the best balance of performance, recording the highest precision (0.95), a substantial recall value (0.88), and superior mAP scores. These outcomes confirm YOLO-v10's advantage in providing reliable and consistent detection compared to YOLO-v9 and YOLO-v11. Overall, the findings underscore the potential of advanced YOLO models in supporting clinical decision-making by enabling faster, more precise, and automated brain tumor detection, thereby contributing to improved diagnostic reliability and patient outcomes.

**Keywords:** YOLO-v9-YOLO-v11, MRI-Images, Brain Tumor Detection



## INTRODUCTION

Brain tumors are unusual growths of cells in the brain that can be either non-cancerous (benign) or cancerous (malignant). When cells in the brain grow uncontrolled and irregularly, it causes brain tumors. (Nadeem et al., 2024). Malignant tumors, such as gliomas, proliferate, can damage nearby brain tissue, and may spread. Usually, benign tumors remain in one place and grow slowly over time. Complications may appear if the cysts enlarge or press on essential organs.(Rastogi et al., 2025a). Brain tumors are either primary, starting in the brain, or secondary (metastatic), spreading from cancers in other body parts. (Dulal & Dulal, 2025). Of all the brain tumors, 28 per cent are malignant and 72 per cent are benign.(Zafar et al., 2024). Symptoms can vary but often include headaches that do not go away, seizures, trouble with memory or thinking, weakness, and vision problems. Diagnosing brain tumors is tough because these symptoms can look like other brain conditions.(Bai, 2025). The Global cancer-related mortality exceeded 10.0 million in 2020 (Aftab, Mehmood, Zhang, et al., 2025).

Between 2023 and 2025, the number of new brain tumor cases worldwide rose from 330,000 to an estimated 342,000, while deaths increased from 265,000 to 272,000 (Siegel et al., 2023). Survival rates are improving slightly: for malignant tumors, the five-year survival rate increased from 33.2% in 2023 to 33.8% in 2025, while non-malignant tumors held a high survival rate of around 92%. These figures underscore the pressing need for early and accurate diagnosis of brain tumors. Brain tumor detection remains a significant challenge in medical imaging due to the brain's complex structure, the wide variety of tumor types, and their irregular shapes and sizes. Magnetic resonance imaging (MRI) is the primary way to identify and assess brain tumors (M et al., 2024). Among numerous technologies, magnetic resonance imaging (MRI) is radiation-free and shows essential information about the tumor's location, size, and type (K et al., 2025; Zulfqar et al., 2024). Deep learning-based automated detection systems have demonstrated outstanding potential to raise brain tumor diagnosis accuracy and efficiency. Among the several models used, the YOLO (You Only Look Once) series stands out mainly because of its fast processing and accuracy in object recognition chores. (Muksimova et al., 2025)(Aftab, Mehmood, Sahibzada, et al., 2025). Limited use with small datasets, having too many incorrect classifications, insufficient live tracking to find and classify tumors correctly, and a lack of extensive collections of labelled tumor data.

This research uses YOLO (You Only Look Once) deep learning models to detect brain cancers from real-time images. This article evaluates the efficacy of YOLO-V9 to YOLO-V11 in analyzing MRI images. The You Only Look Once (YOLO) series editions V9–V11 have considerably enhanced object identification algorithm development. Unique designs and increased training have led to more precise detection, rapid computation, and high dependability in real-time surveillance, autonomous cars, and medical imaging. This literature study examines how YOLO-V9, V10, and V11 models were developed, enhanced, and implemented. It highlights their advances in object identification and the expanding importance of illness and brain tumor research. These strategies can evolve and mold medical imaging for the day when innovative systems can improve patient care. YOLO's approach enables simultaneous and exact identification and localization of objects, as the entire image is processed in a single run through the network. Consequently, this material is ideally suited for medicinal applications due to its uncomplicated manufacturing. Through retraining a specific MRI dataset utilizing meticulously selected anchor boxes and transfer learning, this study attains enhanced accuracy in tumor detection, expedited processing, and consistent performance across various tumor types and imaging modalities. A comprehensive analysis reveals that YOLO-v10 outperforms other models' accuracy and execution time, particularly in detecting tiny or intricately formed tumors. The study improves medical diagnosis by adapting YOLO's proven strengths in autonomous driving and surveillance to healthcare needs.

## LITERATURE REVIEW

Many researchers have investigated the performance of the YOLO (You Only Look Once) family of models, which has considerably advanced real-time object detection. (Baid et al., 2021; Deng et al., 2025; Rivera et al., 2025) . These efforts have significantly improved processing speed, accuracy, and efficiency. However, specific challenges remain unresolved, including detecting tiny objects, improving performance in complex environments, and reducing false positives. Reviewing prior studies, highlighting their limitations, and identifying potential directions for future research form the primary goals of this literature review. (Sajid et al., 2019) combined

YOLOv5 for detection with a 2D U-Net for precise segmentation, using the BTF and BRATS datasets. Their dual-network approach achieved a mAP of 89.5% and a Dice Score of 88.1%, outperforming Faster R-CNN, SSD, and Mask R-CNN. This framework significantly improved both tumor localization and boundary delineation. (Mijwil, 2024) compared CNN architectures, including DenseNet201, Inception-V1, AlexNet, and MobileNetV2, on MRI classification. MobileNetV2 achieved the highest accuracy (96.5%) and sensitivity (96.6%), confirming its practicality for clinical deployment due to its efficiency and robustness. (Yang et al., 2024) enhanced the YOLOv5s architecture by incorporating Atrous Spatial Pyramid Pooling (ASPP) and attention mechanisms such as CBAM and CA. Using glioma and meningioma MRI datasets from Kaggle, the improved YOLOv5s-ASPP model achieved a precision of 93.7%, a recall of 89.1%, and mAP@50 of 92.9%. The feature extraction and lightweight design improvements strengthened its potential for clinical application.

(Alsufyani, 2025) addressed the challenge of accurate and efficient brain tumor detection using deep learning. Employing a Kaggle dataset of 3,903 MRI scans across four categories (glioma, meningioma, pituitary, and no tumor), they compared YOLOv8, YOLO-v9, Faster R-CNN, and ResNet18. YOLO-v9 outperformed the other models, achieving 78.4% accuracy, a mAP of 0.826, and an F1-score of 0.718, demonstrating its suitability for real-time clinical applications. (Alnageeb & M.H., 2025) developed MK-YOLOv8, a lightweight architecture optimized for real-time detection. Enhancements included GhostConv, C3Ghost, and SPPELAN modules, which reduced computational cost while maintaining high performance. The model achieved mAP@0.5 of 99.1% and operated at 62 FPS, excelling in detecting small and extra-small tumors.

(Bin Shabbir Mugdha & Uddin, 2025) developed as a custom CNN framework compared with VGG16, ResNet50, InceptionV3, and AlexNet, using 7023 MRI images. VGG16 delivered the best test accuracy (95.52%), confirming its superior feature extraction capability and robust performance across tumor size and location variations.(Batool & Byun, 2025) captured multi-scale features with parallel paths and feature selection techniques. It achieved 96.03% accuracy on multiclass classification while significantly reducing computational requirements.

(Golkarieh et al., 2025) compared fine-tuned deep learning models, including VGG19, ResNet50, InceptionV3, and EfficientNetV2, for binary and multiclass tumor classification across 17 categories. EfficientNetV2 achieved the highest performance (accuracy = 98.22%, precision = 99.1%, recall = 99.26%, F1 = 99.17%), establishing its suitability for clinical diagnostics and motivating future 3D extensions. (Hezil et al., 2025) combined Fuzzy C-Means clustering with LSTM networks for tumor segmentation. The model achieved Dice scores of 91.5–91.8%, showing robustness while reducing reliance on large labelled datasets. (Hosny et al., 2025) integrated DenseNet121 and InceptionV3 with Grad-CAM interpretability tools. Achieving 99.02% accuracy, 98.75% precision, 98.98% recall, and 98.86% F1-score, this approach demonstrated both high diagnostic accuracy and clinical transparency. (Kang et al., 2025) introduced PK-YOLO, a novel YOLO-based architecture that integrated domain knowledge via the SparK RepViT backbone and introduced a new loss function (Focaler-IoU). Applied to multiplanar MRI slices, PK-YOLO achieved state-of-the-art performance, particularly for small tumor detection across axial, coronal, and sagittal planes. While computationally more demanding, it outperformed other YOLO and DETR-based models. (Monisha & Rahman, 2025) proposed a privacy-preserving federated learning framework that integrated YOLO-v9, YOLO-v10, and YOLO-v11 for brain

tumor detection in MRI data. Their dataset included 10,000 labelled T1-weighted contrast-enhanced scans of gliomas, meningiomas, and pituitary tumors. The federated approach enabled training across multiple healthcare facilities while maintaining data privacy. YOLO-v11 achieved the strongest performance with a precision of 0.90 and mAP@0.5 of 0.90, effectively detecting complex tumors while safeguarding sensitive medical data.

(Mathivanan et al., 2025) combined CNNs with graph convolutional networks (GCNs) to refine segmentation. The model improved Dice scores and classification accuracy by enforcing spatial consistency across slices, demonstrating robustness to noise and improved boundary delineation. Another dual-task framework (AlShowarah, 2025) performed simultaneous classification and segmentation using a shared CNN backbone with an attention-based fusion module. It achieved competitive Dice scores and strong classification performance, outperforming single-task baselines.

(Nahiduzzaman et al., 2025) proposed a hybrid explainable framework that combined CLAHE preprocessing, a lightweight PDSCNN for feature extraction, and a ridge regression-enhanced extreme learning machine (RRELM) classifier. It achieved 99.35% precision, 99.30% recall, and 99.22% accuracy, while maintaining interpretability through SHAP explanations (Onaizah et al., 2025) used CNN feature extraction followed by attention-based fusion across slices, optimizing segmentation and classification. Evaluations on BraTS datasets confirmed robust accuracy and effective false-positive reduction.

(Pande & Chaki, 2025) proposed for robust brain tumor classification under noisy and scarce data conditions. It fused features from DenseNet121 and ResNet101, reduced redundancy using PCA, and employed a Random Forest classifier. The model was evaluated on multiple datasets and achieved over 90% accuracy, demonstrating robustness and outperforming single-model baselines. (Pasunoori et al., 2025) introduced a hybrid deep learning model that combined YOLO11n for detection and SAM2 for segmentation. Using 834 MRI images from the Roboflow platform, their model integrated C2PSA blocks for spatial attention and SAM2's memory-attention mechanism for improved segmentation. The framework achieved a Dice Score of 96.39% and IoU of 93.03%, confirming its strong alignment with ground truth segmentation masks.

(Rastogi et al., 2025) applied fine-tuned transfer learning with InceptionResNetV2, VGG19, Xception, and MobileNetV2 models. Xception achieved the highest accuracy of 96.11% in distinguishing tumor from non-tumor images, highlighting the effectiveness of transfer learning for clinical diagnostics. (Rasool et al., 2025) integrated attention-guided fusion modules for brain tumor grading and segmentation. Using hybrid loss functions, it achieved competitive Dice scores and high classification accuracy for tumor grading, outperforming standard CNN baselines. (Sokea & Marina, 2025) integrated GANs with CNNs to address dataset limitations. GANs augmented MRI datasets, while CNNs performed classification. The approach improved precision, sensitivity, and specificity, showing strong potential for clinical applications where data scarcity is challenging.

(Shoaib et al., 2025) combined DenseNet201, EfficientNetB5, and InceptionResNetV2 with PCA feature reduction and traditional classifiers (SVM, MLP, GNB). DenseNet201 with SVM/MLP achieved near-perfect accuracy, supported by 5-fold cross-validation and visual evidence of robust class separability. (Taha et al., 2025) explored tumor detection using a hybrid dataset of over 39,000 MRI images from three public

repositories. The models evaluated included YOLOv8, YOLO-v11, and a custom CNN. Results showed that YOLO-v11 achieved the highest accuracy (99.56%), closely followed by YOLOv8 (99.49%). These findings confirm the models' effectiveness in supporting high-precision and real-time diagnostics. (Wekalao et al., 2025) approached to a graphene-based surface plasmon resonance meta-surface sensor was introduced using terahertz technology for early brain tumor detection. Incorporating graphene, gold, and methylammonium lead halide on a $SiO_2$ substrate with a T-shaped resonator, the design achieved a sensitivity of 1538 GHz/RIU, a figure of merit of 29.586 $RIU^{-1}$, and a detection limit of $5.1 \times 10^{-2}$. Coupled with XGBoost regression, the sensor demonstrated 98–100% predictive accuracy, offering a promising non-invasive diagnostic tool. (Wahidin & Kosala, 2025) evaluated advanced YOLO variants for brain tumor detection. Their findings showed that YOLO11m provided the highest accuracy, while YOLOv8m achieved the fastest inference speed. Hyperparameter tuning further improved performance, confirming YOLO's adaptability to clinical workflows.

## Materials and Methods

In this study, as shown in Table 1, we evaluate the performance of YOLO-V9, YOLO-V10, and YOLO-V11 for brain tumor detection using MRI images. The process involves systematic steps, including data collection, image preprocessing, model training, and performance assessment. Our primary focus is to examine the efficiency of these models within the context of medical imaging. By adhering to a consistent and well-structured methodology, we ensured the reliability and accuracy of the results.

The workflow, illustrated in the diagram, begins with the collection of brain MRI images, followed by preprocessing steps such as normalization, noise reduction, resizing, and augmentation techniques like scaling, flipping, and mosaic transformations. The dataset is then divided into training and validation subsets. Model training involves specific configurations, including epochs, batch size, optimizer, momentum, and learning rate. Following training, the models are evaluated using standard performance metrics such as mAP, precision, recall, and F1-score. The outcomes are finally presented through visualizations of training curves and detection outputs highlighting tumor-localized MRI scans.

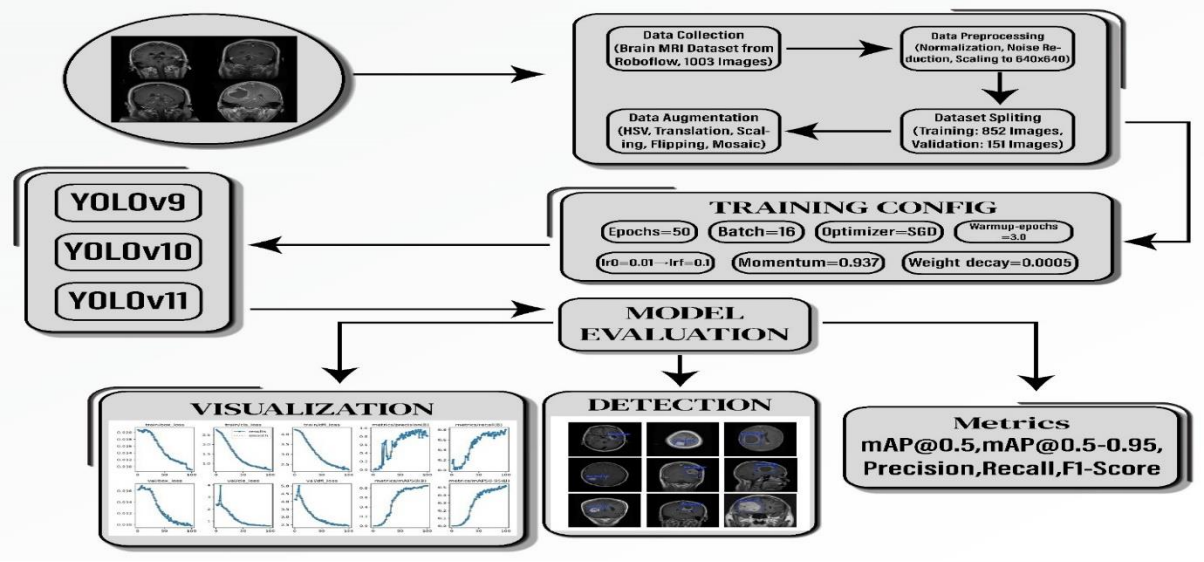


**Figure 1:**
**Workflow of Brain Tumor Detection Using YOLO-v9–YOLO-v11 on MRI Images.**

## Data Collection

Brain MRI dataset taken from Roboflow, consisting of 1003 images, each suitable for detecting brain tumors. For Training purposes, 852 images were used, and 151 images were utilized for validation. The images are automatically put together for the model to see various tumor types, and each one is scaled to a standard size of 640x640 pixels.

## Data Preprocessing

Before analyzing brain tumors, pre-processing is necessary to make the MRI data more consistent and of higher quality. The output is standardized, noise-reducing, and adds to various data inputs as part of these steps. This makes finding and identifying tumors easier and makes the tests more accurate, dependable, and usable in more situations. This concludes that pre-processing sets up the proper structure for AI-based study of brain tumors.

## Data Augmentation

Data augmentation may train a model on diverse patterns by converting data into the HSV color space, translating, scaling, and flipping. As in actual scans, changing these conditions alters picture brightness, location, and angle. Adjusting color, saturation, and value in photographs lets the model accommodate scans from more sources and scenarios, while adjusting translation and size scales imitate tumor movement and placement. Our augmentations allow the model to apply to more instances without changing critical medical qualities, even without mix-up or copy-paste approaches to prevent overfitting. These standard setups between YOLO versions allow for an organized and extensive assessment of how each version identifies tumors in various scans.

## Loss Functions

The YOLO models (YOLO-v9 to YOLO-v11) optimize a composite loss function combining box regression, classification, and distribution focal loss (DFL):

$$L_{total} = \lambda_{box}L_{box} + \lambda_{cls}L_{cls} + \lambda_{dfl}L_{dfl}$$

where$\lambda_{box} = 0.05, \lambda_{cls} = 0.3, and \lambda_{dfl}$.

### *Box Loss*

$$L_{box} = 1 - GloU\left(B, B^{\wedge}\right) = 1 - \left(\frac{|B \cap B^{\wedge})|}{|B \cup B^{\wedge})|} - \frac{|C\backslash(B \cup B^{\wedge})|}{|C|}\right)$$

Where $B$ Is the predicted bounding box,$B^{\wedge}$ Is the ground truth, and C is the smallest enclosing box.

## Classification Loss

$$L_{cls} = -\frac{1}{N}\sum_{i=1}^{N}\left[y_i log(y^{\wedge}_i) + (1 - y_i) log\left(1 - y_i^{\wedge}\right)\right]$$

Where $y_i \epsilon \{0,1\}$ is the actual label, $y_i^{\wedge} \epsilon \{0,1\}$ is the predicted probability, and $N$ Is the number of samples.

## Distribution Focal Loss

$$L_{dfl} = -\sum_x SoftLable(x)\log\left(Pred(x)\right)$$

Where SoftLabel $(x)$ and Pred$(x)$ are the soft label and predicted probability distributions, respectively.

## Learning Rate Schedule

The learning rate is adjusted from an initial value of 0.01 to a final value of 0.1 over 100 epochs, as specified in Table 1. The learning rate at epoch $t$ follows a cosine annealing schedule:

$$\eta_t = \eta_{final} + \frac{1}{2}\left(\eta_{initial} - \eta_{final}\right)\left(1 + cos\left(\frac{t}{T}\pi\right)\right)$$

Where $\eta_{initial} = 0.01, \eta_{final} = 0.01 \times 0.1 = 0.001, T = 100\ epochs, and\ t\epsilon[0, T]$.

## Warmup Strategy

During the first three epochs, a warmup strategy gradually increases the learning rate and adjusts momentum. The warmup learning rate at epoch $t_w$ is:

$$\eta_{warmup}(t_w) = \eta_{initial} \cdot \frac{t_w}{T_w}, \qquad t_w\ \epsilon\ [0, T_w]$$

The warmup momentum is:

$$m_{warmup}(t_w) = m_{initial}\ + (0.937 - m_{initial}).\frac{t_w}{T_w}$$

Where $m_{initial}\ = 0.8\ (Table1), and\ 0.937$ is the final momentum.

## Experimental Setup

To get better results, we set up specific training settings and used several different augmentation methods on YOLO-v9 to YOLO-v11 models that were made to find brain tumors. Table 1 provides a detailed overview of all training configurations and augmentation settings used in this study.

Warmup gradually increases learning rate throughout the initial half of training, allowing the model to handle complex tumor features without the full benefit of quicker learning. Different momentum and bias terminal rates create a steady method for evaluating data basics before particular learning rates. Loss function configurations provide values to box and classification losses, so the model can reliably locate tumors near the actual border and classify each box. With this balance, the model learns to focus on localization and detection when trained, giving medical imaging specialists confidence.

**Table 1.**

**YOLO-V9–YOLO-V11 training configuration parameters and augmentation techniques for brain tumor identification.**

| Category | Parameter | Value/Description |
|---|---|---|
| **Training Setup** | Epochs | 100 |
| | Batch Size | 16 |
| | Optimizer | SGD |
| | Visualizations | Enabled |

| | | |
|---|---|---|
| **Learning Rate & Optimisation** | Initial Learning Rate | 0.01 |
| | Final LR Factor | 0.1 |
| | Momentum | 0.937 |
| | Weight Decay | 0.0005 |
| **Warmup Strategy** | Warmup Epochs | 5.0 |
| | Warmup Momentum | 0.8 |
| | Warmup Bias LR | 0.1 |
| **Loss Function Configuration** | Box Loss (box) | 0.05 |
| | CL | 0.3 |
| | DFL | SoftLabel(x)×log (Pred(x)) |
| **Data Augmentation** | HSV (h, s, v) | 0.015, 0.7, 0.4 |
| | Translation | 0.2 |
| | Scaling | 0.5 |
| | Flipping (flip) | 0.5 |
| | Mosaic | 1.0 |

## Architecture of the YOLO-v9 Model

Figure 2 shows the architecture of YOLO-v9, which focuses on identifying objects and extracting features from bottom to top. Through Programmable Gradient Information (PGI) and Multi-Level Auxiliary Supervision, the system ensures that training is stable and improves how gradient information is used. An object detection system is built after the input picture (640x640x3) goes through the GLEAN backbone. Then, the PANet, SPF, and Attention Mechanism modules are applied to help the system better understand the context. To detect objects, a network uses anchor-based predictions, and after that, the predictions undergo classification and regression steps with NMS applied to remove repetitive boxes. By keeping speed and accuracy equal, the architecture makes sure objects are recognized effectively and precisely.

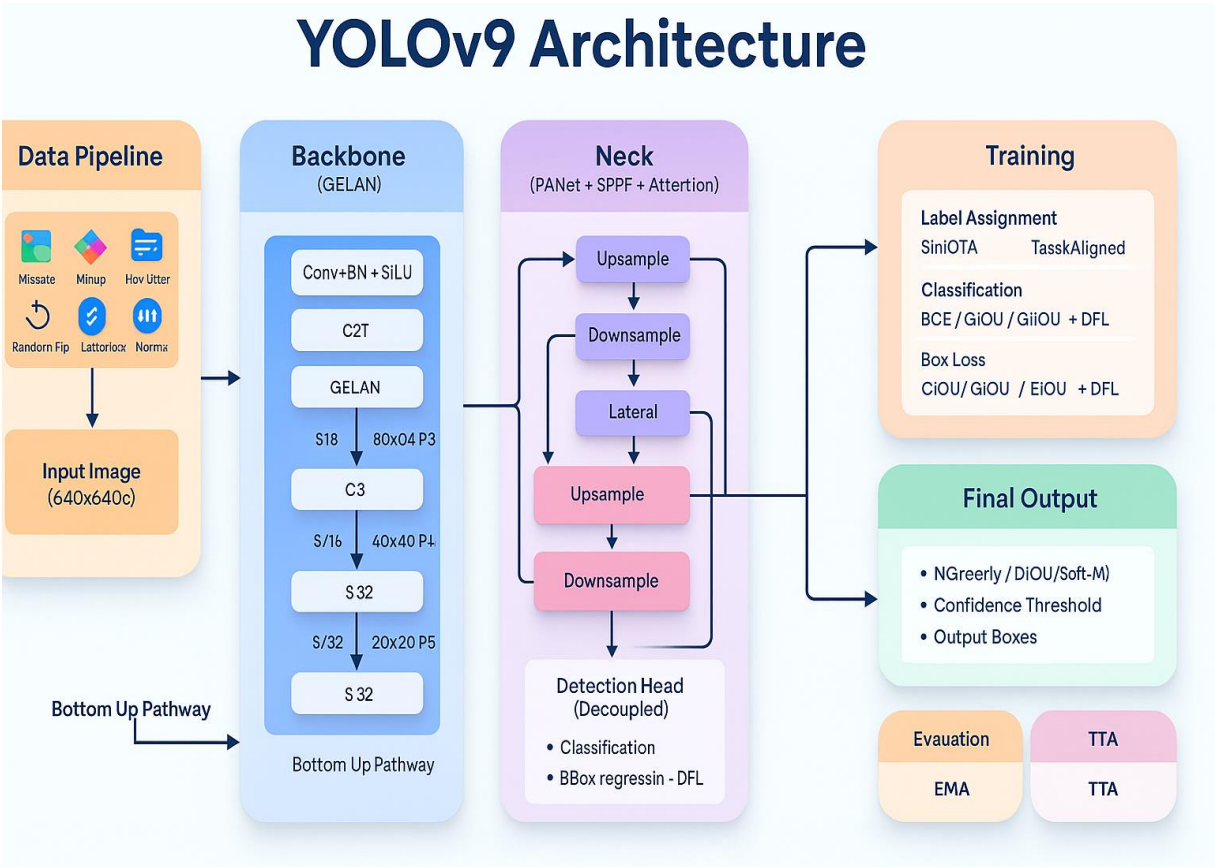


**Figure 2:**
**Architecture of YOLO-v9**

## Architecture of the YOLO-v10 Model

Figure 3 describes the architecture of YOLO-v10 with its unique design changes. YOLO-v10 achieves better performance in object detection than previous versions. Transformer-Lite is the backbone for extracting features and building a smaller overall architecture. Because of the dual detection head system, which is a "One-to-Many" head for supervised training and a "One-to-One" head for inference without NMS, improves accuracy and speed. It is possible to use effective multi-scale detection because PANet links features in an improved manner using attention strategies. The One-to-One head can learn from the One-to-Many head by always using a dual assignment routine, ensuring correct predictions and reliable training routines. The direct outputs from the One-to-One head of YOLO-v10 enable it to process quickly and still be accurate, as it does not need Non-Maximum Suppression.

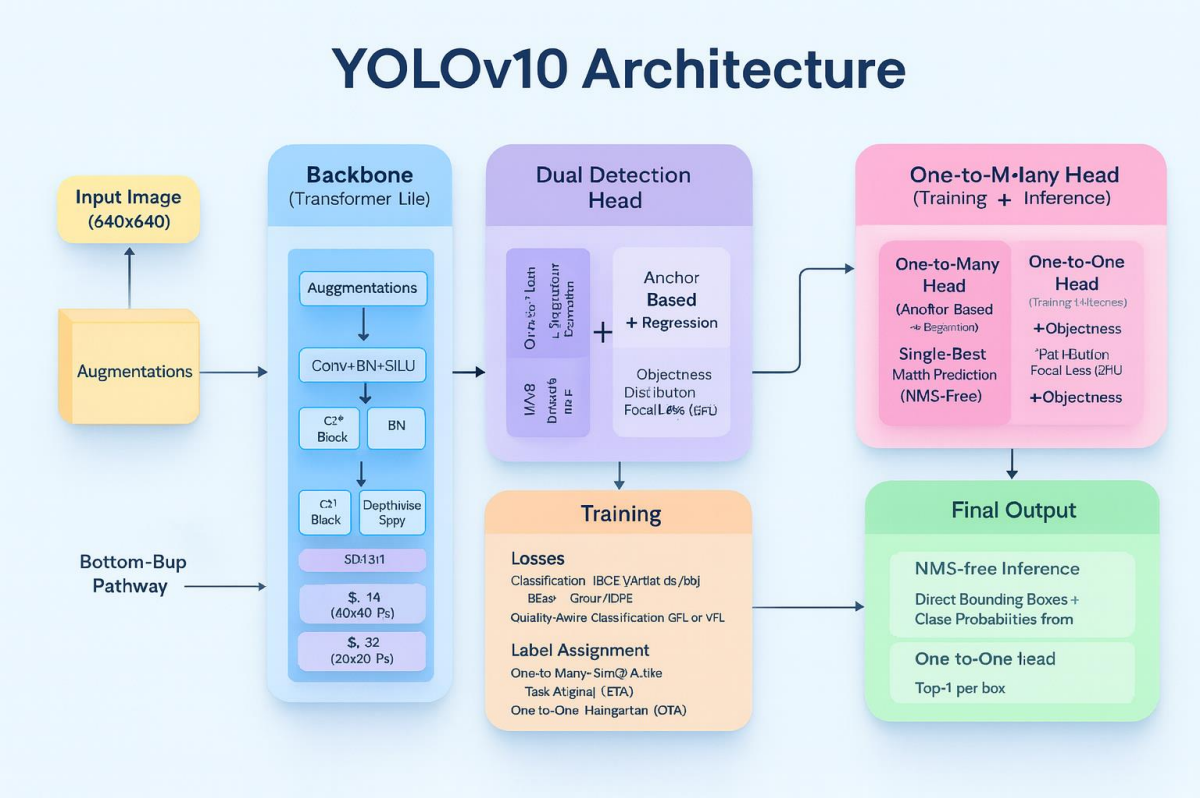


**Figure 3.**
**Architecture of YOLO-v10**

## Architecture of the YOLO-v11 Model

Figure 4 illustrates the architecture of the YOLO-v11 model, which is systematically organized into three major components: the backbone, the neck, and the head. Each of these plays a distinct but complementary role in the detection pipeline. The backbone is responsible for extracting hierarchical features from the input image. It processes the data through convolutional layers, C3×2 blocks, and SCDown layers, enabling the model to capture low-level and high-level information across multiple scales (P3 to P5). To further strengthen its representation power, additional modules such as C2fSA and SPPF are integrated, improving feature extraction efficiency by enhancing spatial attention and context aggregation. Once the features are extracted, the neck performs feature aggregation and multi-scale fusion. It adopts PANet-style pathways, using up-sampling, down-sampling, and cross-scale concatenation to combine semantic richness and spatial precision effectively. This

process allows the network to refine and align features across different resolutions. Furthermore, including C3K2 and C2fSA layers strengthens the neck by improving the balance between localization accuracy and semantic understanding. The final stage, the head, performs detection at multiple scales (P3, P4, and P5). Unlike earlier YOLO versions that rely on conventional Non-Maximum Suppression (NMS), YOLO-v11 incorporates one-to-one prediction and supports optional one-to-many training. This innovation reduces redundancy in bounding box predictions while maintaining flexibility during training. As a result, the model can generate cleaner outputs with improved detection consistency. The figure highlights how the YOLO-v11 architecture leverages advanced modules and cross-scale design strategies to deliver accurate, efficient, and robust object detection performance. The subsequent figures provide a more detailed layer-wise visualization of the entire network.

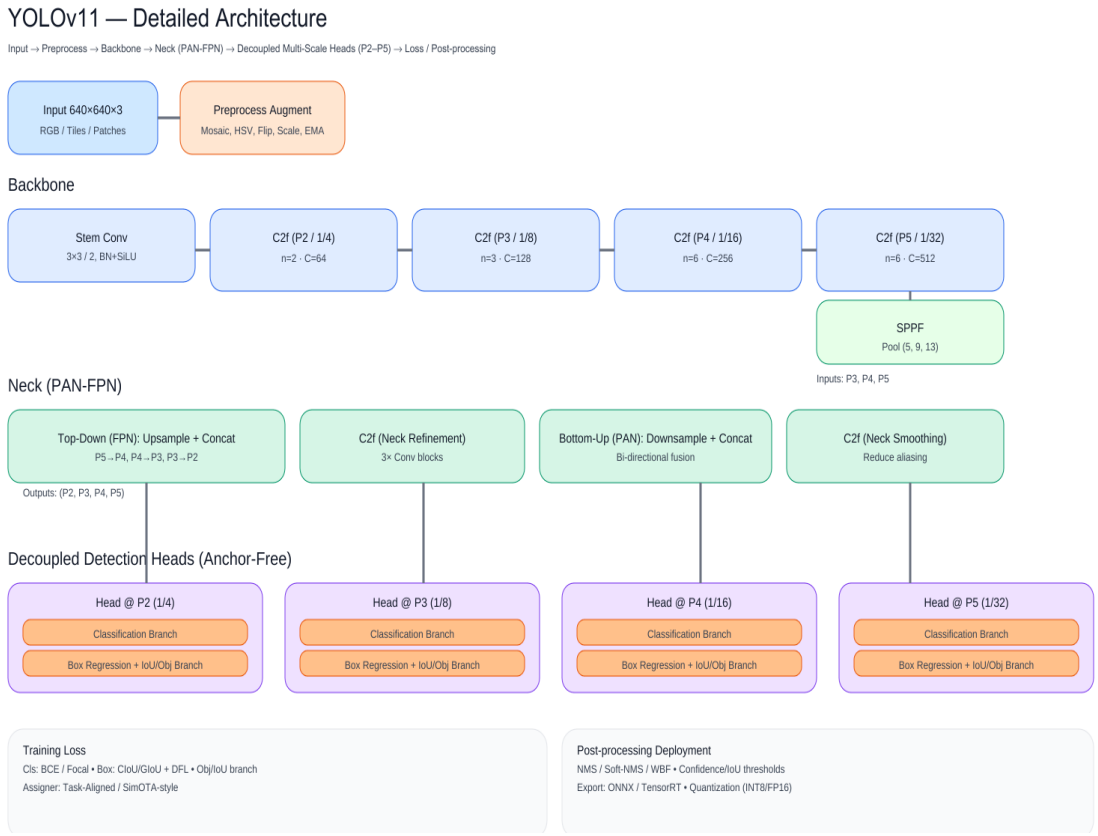


**Figure 4.**
**Architecture of YOLO-v11**

## Performance Metrics

We employed a range of established evaluation metrics to assess the models' performance on brain tumor datasets. By analyzing the number of True Positives (TP), True Negatives (TN), False Positives (FP), and False Negatives (FN) for brain tumor detection, we can calculate various performance metrics that provide insights into how well the model detects tumor-affected brain tissue. These metrics include: Recall or sensitivity measures a model's ability to correctly identify all positive cases, such as patients with brain tumors and their specific types. It is calculated as the ratio of true positives (TP), correctly identified tumor cases, to the total number of tumor cases. This metric reflects how effectively the model detects all existing tumors.

$$Recall = \frac{True\ Positive}{True\ Positive\ +\ False\ Positive}$$

Precision measures the model's accuracy in correctly classifying positive cases, such as patients with brain tumors and their specific types. It indicates the proportion of patients identified by the model as having a tumor (true positives, TP) who have a tumor. This metric reflects the reliability of the model's optimistic predictions.

$$Precision\ = \frac{True\ Positive}{True\ Positive\ +\ False\ Positive}$$

The F1-score provides the harmonic mean of precision and recall, offering a balanced assessment of a model's performance in identifying tumors and achieving overall classification accuracy.

$$F1 - Score\ =\ 2\ \cdot \frac{Precision.Recall}{Precision+Recall}$$

The Intersection over Union (IoU) metric evaluates the accuracy of YOLO-v9 to YOLO-v11 in localizing brain tumors in MRI images. It measures the ratio of the overlap (intersection) to the combined area (union) of predicted and actual tumor bounding boxes. Higher IoU scores indicate better precision in tumor localization.

$$IoU\ = \frac{|B \cap B\hat{})|}{|B \cup B\hat{})|}$$

The mean Average Precision at IoU 0.5 (mAP@0.5) is a key metric for evaluating object detection models like YOLO-v9 to YOLO-v11 in brain tumor detection. It is calculated as the average precision across all classes, where precision is integrated over recall levels from 0 to 1 for each class, where $N_c$ Is the number of classes, and ( p(r) is the precision-recall curve at an IoU threshold of 0.5. This metric reflects the model's accuracy in detecting and classifying brain tumors.

$$mAP@0.5 = \frac{1}{N_c}\sum_{c=1}^{N_c}\int_0^1 p(r)dr$$

The mean Average Precision across IoU thresholds from 0.5 to 0.95 (mAP@0.5:0.95) evaluates the performance of object detection models, such as YOLO-v9 to YOLO-v11, in detecting and localizing brain tumors in MRI images. This metric averages the mAP scores calculated at IoU thresholds ranging from 0.5 to 0.95, in increments of 0.05 (i.e., 0.5, 0.55, 0.6, ..., 0.95). Each mAP@IoU represents the average precision for a specific IoU threshold across all classes, comprehensively assessing the model's ability to balance detection accuracy and localization precision for brain tumor identification.

$$mAP@0.5{:}\,0.95 = \frac{1}{10}\sum_{IoU=0.95}^{0.95} mAP@IoU$$

## RESULTS AND DISCUSSIONS

A detailed summary of the assessment measures used to compare the performance of YOLO-V9 to YOLO-V11 in MRI-based brain tumor detection is presented. The evaluation methodology covers the main areas of model performance. Loss is used to assess classification performance, and Distribution Focal Loss (DFL) improves localization by addressing label distribution smoothness. Additional evaluations using IoU and AP reinforce the fine-grained nature of the precision-recall curve. mAP is used

to assess how effective the models are at IoU ≥ 0.5 and a range of detection thresholds (0.5:0.95). Tumor detection reliability is further analyzed using precision, recall, and F1-score, which indicate how well the models identify tumors. To ensure real-time applicability, efficiency is measured through FPS (frames per second) and NMS (Non-Maximum Suppression) time, both essential for instant diagnostic use. This combination of predictive and efficiency-based evaluations ensures that the models are assessed for accuracy and practical deployment in medical applications.

Table 2 compares the effectiveness of the three models. YOLO-V10 delivers the best overall performance, achieving the highest precision (0.953), strong recall (0.952), and an F1-score of 0.917. These results demonstrate YOLO-V10's ability to provide high accuracy while balancing precision and recall. YOLO-V11 achieves the highest recall (0.910), making it more effective at detecting tumors. However, its F1-score (0.865) reflects a trade-off, as increased sensitivity comes at the expense of lower precision and slightly reduced overall balance. YOLO-V9 shows moderate but consistent performance across all metrics, reinforcing its reliability as a baseline model.

**Table 2.**
**Performance Metrics of YOLO-v9 to YOLO-v11**

| Model | Precision | Recall | mAP@0.5 | mAP@0.5:0.95 | IoU | F1-Score |
|---|---|---|---|---|---|---|
| **YOLO-v9** | 0.88 | 0.87 | 0.913 | 0.56 | 0.87 | 0.87 |
| **YOLO-v10** | 0.95 | 0.88 | 0.95 | 0.64 | 0.91 | 0.91 |
| **YOLO-v11** | 0.82 | 0.91 | 0.94 | 0.63 | 0.86 | 0.86 |

This graph uses MRI images to compare the performance metrics of YOLO-v9, YOLO-v10, and YOLO-v11 for brain tumor detection. YOLO-v10 demonstrates the best overall results, achieving the highest precision (0.95) and a strong balance across recall, IoU, and F1-score. YOLO-v11 has the highest recall (0.91), making it more sensitive to tumor detection but at lower precision. YOLO-v9 shows moderate but consistent performance across all metrics, establishing it as a reliable baseline. The mAP@0.5 and mAP@0.5:0.95 scores indicate steady improvements from YOLO-v9 to YOLO-v11, highlighting advancements in localization accuracy. YOLO-v10 offers the most balanced and clinically applicable performance among the three models.

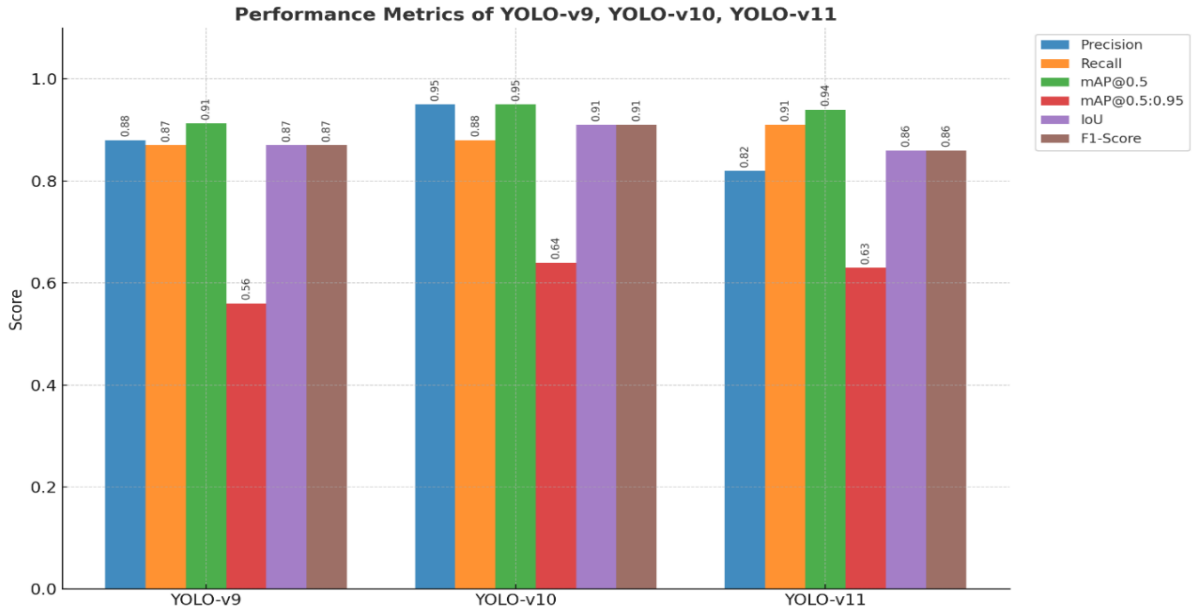


**Figure 5.**
**Overall Results of Brain Tumor Detection Metrics Across YOLO-v9 to YOLO-v11**

Figure 5 shows the graphical representation of training and validation metrics, demonstrating how well YOLO-V9 detects brain cancers. Box loss shows a steady decrease during training and validation, suggesting the program learned well where the tumors are located. The Dependability of the model is established by the high rate of correct detections, as well as mAP50, and an accuracy of above 0.8. The mAP50-95, which measures how well a system works using IoU values from 0.5 to 0.95, is valued for its stability and strength at all detection thresholds. They prove that YOLO-V9 performs medical imaging effectively by balancing how fast it runs with how diagnostic it is, which is essential in this area. Performance Analysis of YOLO-v10 in Brain Tumor Detection.

Figure 6 presents the graphical representation of training and validation metrics, indicating the performance of YOLO-v10 in identifying brain tumors. Tumor localization improves as the box loss decreases, indicating that bounding box regression becomes more accurate. The validation results confirm that the classifier can detect tumors more accurately.

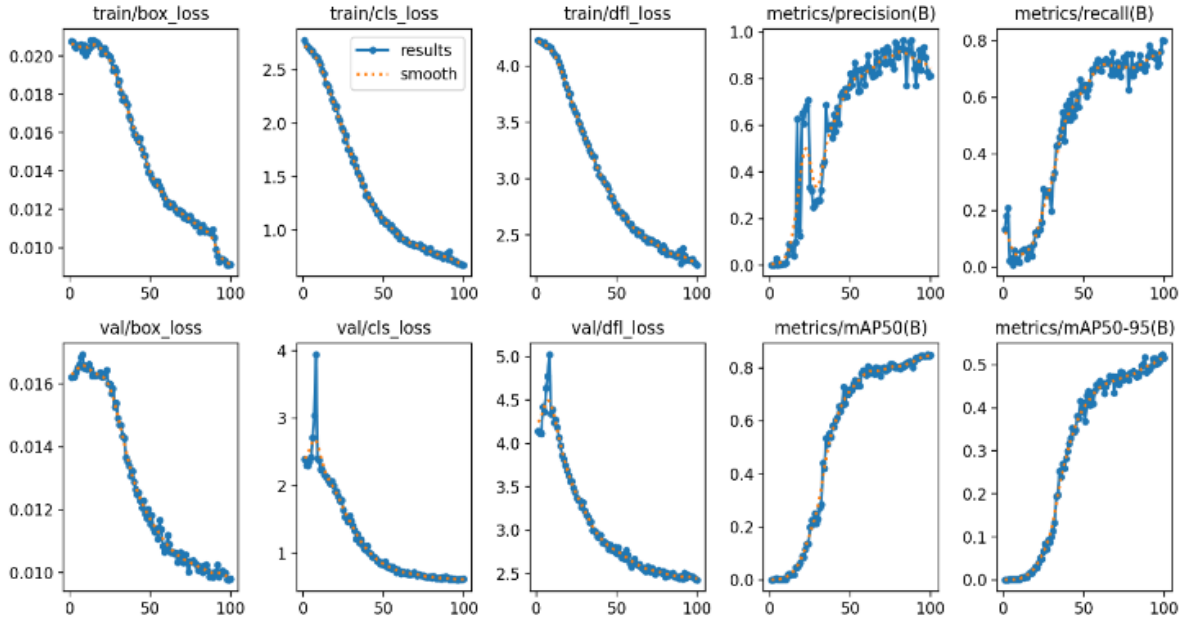


**Figure 6.**
**YOLO-v9 Results of Training and Validation Metrics**

The model demonstrates a strong ability to detect tumors with precision, recall, and mAP@50 reaching high results. Also, the model's steady performance against different criteria is confirmed by the stable mAP@50-95 numbers, between IoU ranges of 0.5 and 0.95. The outcomes demonstrate that YOLO-v10 has improved speed and accuracy, making it perfect for medical image processing. Performance Analysis of YOLO-v11 in Brain Tumor Detection.

Figure 8 demonstrates how YOLO-v11 trains and validates over 100 epochs. Box loss, classification loss (cls_loss), and distribution focal loss (dfl_loss) show a regular decrease during training and validation. Even more interesting, the box loss falls to 0.10 for validation and 0.050 for training. Further, the accuracy and recall of bounding box detection rise to 0.8 and 0.6, respectively. At the same time, with mAP at 0.8 and 0.5, the results indicate a clear upturn when IoU thresholds are 0.50 and 0.50:0.95, respectively. The smooth orange lines confirm the model's progress, demonstrating that YOLO-v11 does well in finding objects in images.

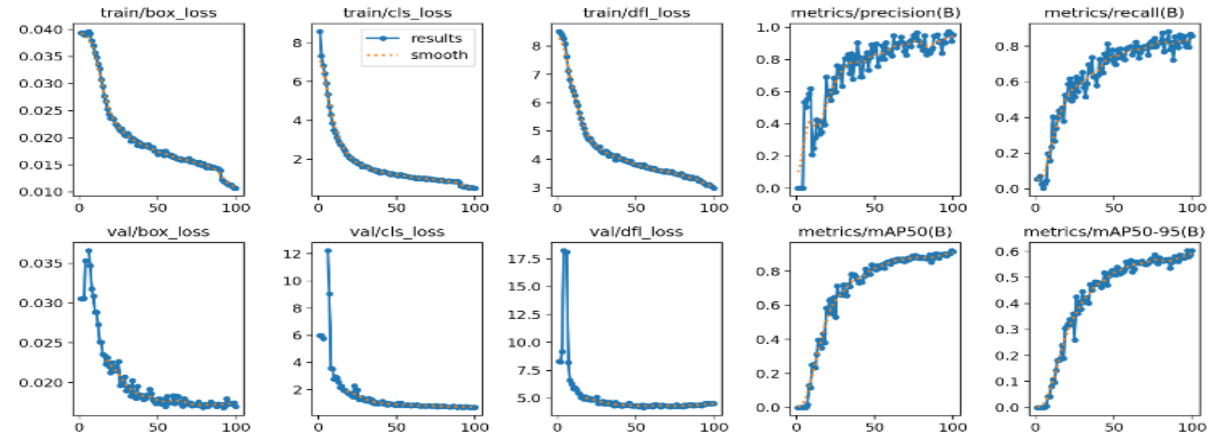


**Figure 7.**
**YOLO-v10 Results of Training and Validation Metrics**

Figure 8 demonstrates how YOLO-v11 trains and validates over 100 epochs. Box loss, classification loss (cls_loss), and distribution focal loss (dfl_loss) show a regular decrease during training and validation. Even more interesting, the box loss falls to 0.10 for validation and 0.050 for training. Further, the accuracy and recall of bounding box detection rise to 0.8 and 0.6, respectively. At the same time, with mAP at 0.8 and 0.5, the results indicate a clear upturn when IoU thresholds are 0.50 and 0.50:0.95, respectively. The smooth orange lines confirm the model's progress, demonstrating that YOLO-v11 does well in finding objects in images.

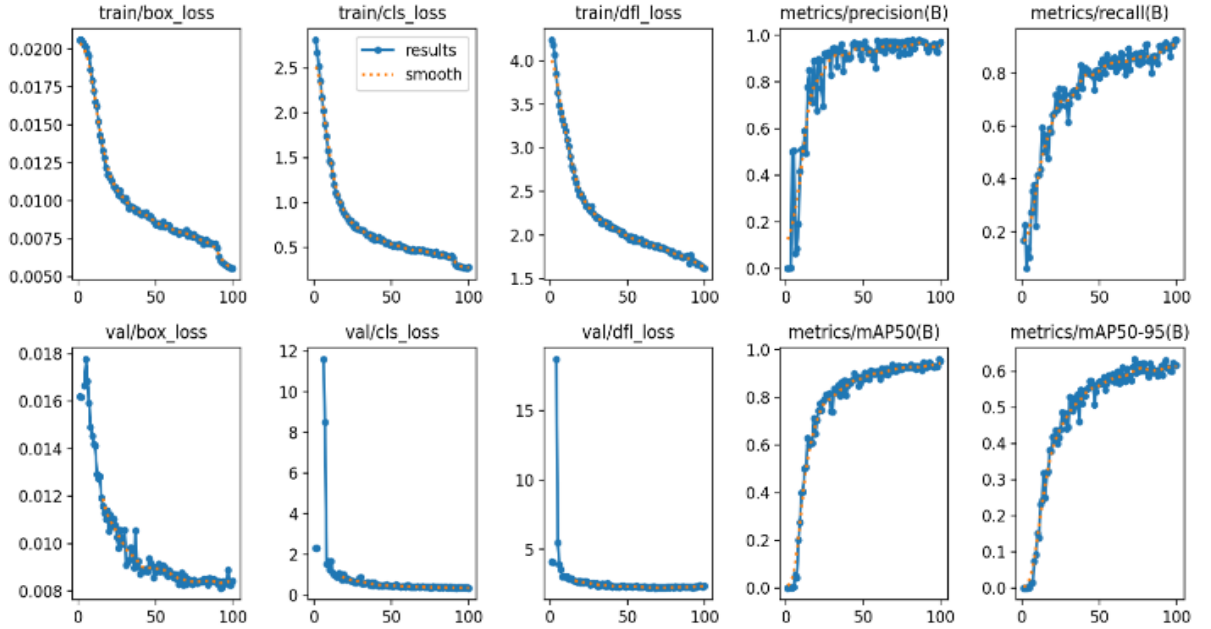


**Figure 8.**
**YOLO-v11 Results of Training and Validation Metrics**

Figure 9 proves that the YOLO-v9 to YOLO-v11 models properly find brain tumors on many MRI images. The tumor spots are represented by blue boxes labelled brain tumor, and confidence ranks from 0.72 to 0.92 are included. The pictures display axial, coronal, and sagittal planes, among other anatomical perspectives, proving the models' capacity to precisely locate tumors in various orientations. These findings highlight the YOLO-v11 model's enhanced resilience and detection accuracy in detecting brain cancers compared to its predecessors.

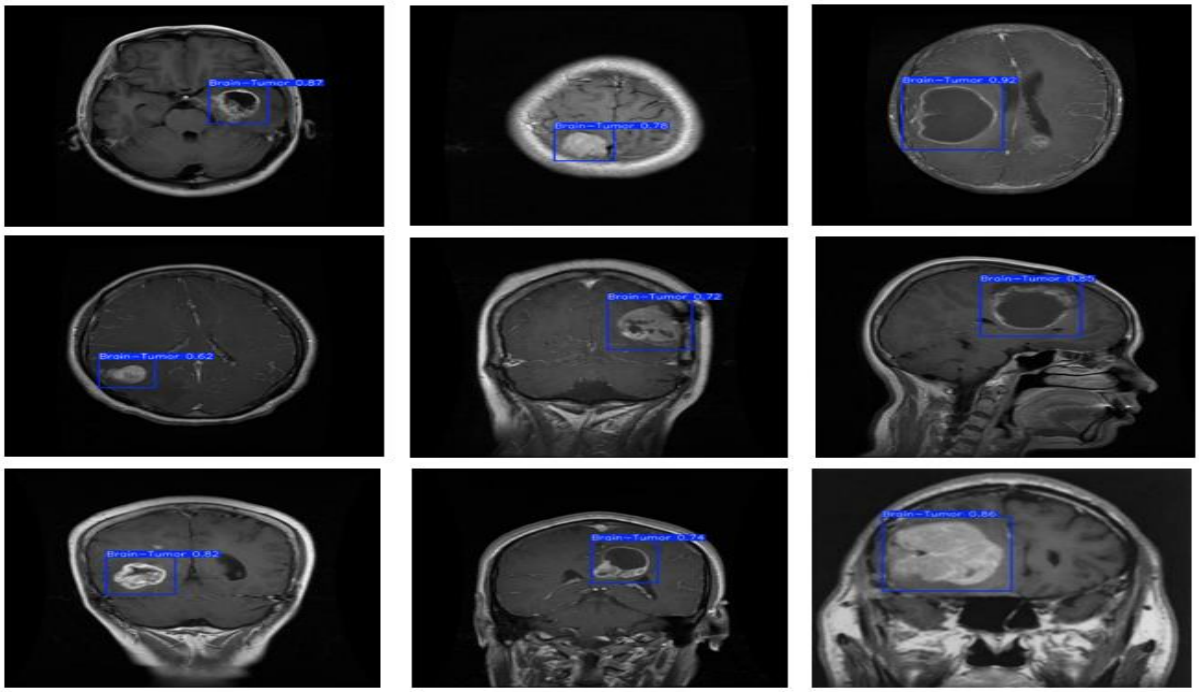

**Figure 9.**
**Detection Results of Brain Tumors in MRI Images using YOLO-v9 to YOLO-v11**

The table summarizes brain tumor detection and classification studies using various MRI datasets, focusing on gliomas, glioblastomas, and metastases. It highlights the datasets used (e.g., BraTS, TCGA, Kaggle), analyzed features (MRI texture, intensity, radiomic properties), and methods (CNNs, ensemble learning, radiomics). Detection rates range from 83.0% to 89.5%, with observations noting challenges like limited generalizability, variable multi-class performance, and dataset-specific effectiveness. The studies demonstrate advancements in tumor identification but face issues with subtype differentiation and robustness across diverse datasets.

**Table 3.**
**Comparative summary of existing studies in medical imaging**

| Reference | Dataset | Method | Performance |
|---|---|---|---|
| (Batool & Byun, 2025) | MRI datasets (multi-class, Kaggle & institutional) | Multi-Path CNN with feature selection | 92.25% (all features), 96.03% (selected features) |
| (Hezil et al., 2025) | BraTS benchmark dataset | Fuzzy C-Means + LSTM hybrid model (segmentation + classification) | 91.8%–91.5% Dice similarity |
| (Mijwil, 2024) | >3000 MRI scans (Kaggle) | CNNs (DenseNet201, InceptionV1, AlexNet, MobileNetV2) | 96.5% accuracy (MobileNetV2 best) |
| (Hosny et al., 2025) | Public MRI dataset (meningioma, glioma, pituitary) | Ensemble (DenseNet121 + InceptionV3 + Grad-CAM explainability) | 99.02% accuracy |
| (Mathivanan et al., 2025) | Br35Hc, BraTS, Kaggle MRI datasets | Brain Tumor Detection Network (BTDN) + Secure-Net | 99.68% (Br35Hc), 98.81% (BraTS), 95.33% (Kaggle) |
| (AlShowarah, 2025) | Brain MRI datasets (public, multiple splits) | CNN feature extraction (VGG-19, AlexNet) + KNN/SVM/RF | 99.1% accuracy |
| (Rasool et al., 2025) | MRI dataset (tumor vs. non-tumor classification) | CNN-TumorNet + LIME explainability | 99% accuracy |

# CONCLUSION

This study presents a robust sequential deep learning framework for brain tumor identification and segmentation, leveraging advanced YOLO variants (YOLO-v9, YOLO-v10, and YOLO-v11) integrated with an effective preprocessing pipeline. The preprocessing steps, including intensity normalization, histogram equalization, and edge-based ROI extraction, significantly enhanced MRI slices' quality and diagnostic relevance. Through systematic evaluation, YOLO-v9, YOLO-v10, and YOLO-v11 each demonstrated medical-grade performance, with distinct strengths across different diagnostic tasks. YOLO-v9 achieved a precision of 0.88, a recall of 0.87, mAP@0.5 of 0.913, mAP@0.5:0.95 of 0.56, IoU of 0.87, and an F1-Score of 0.87. These results indicate its strength in accurate tumor boundary delineation, making it valuable in segmentation-oriented clinical workflows where contour precision is essential for surgical planning. YOLO-v10, in contrast, offered the most balanced performance across evaluation metrics, reaching a precision of 0.95, a recall of 0.88, mAP@0.5 of 0.95, mAP@0.5:0.95 of 0.64, IoU of 0.91, and an F1-Score of 0.91.

This balance highlights its suitability for general diagnostic applications where it is critical to minimize false positives and negatives. Finally, YOLO-v11 excelled in sensitivity, achieving the highest recall of 0.91, with a precision of 0.82, mAP@0.5 of 0.94, mAP@0.5:0.95 of 0.63, IoU of 0.86, and an F1-Score of 0.86. This makes YOLO-v11 particularly effective in high-stakes diagnostic scenarios such as early screening, where missing a tumor could lead to severe consequences, even if it comes at the expense of a slight drop in precision. The efficient architecture and training strategy of these YOLO variants ensured robust performance across diverse imaging conditions, while maintaining inference speeds suitable for real-time deployment in hospital systems without diagnostic delays.

Nevertheless, several limitations were identified. The evaluation was restricted to two publicly available datasets, which may not fully represent the variability of real-world clinical imaging across diverse populations and acquisition settings. The reliance on 2D MRI slices limited the ability of the framework to capture full volumetric spatial context, which could be addressed by incorporating 3D MRI analysis. Furthermore, the models were not tested on additional imaging modalities such as CT or PET, often integral to multidisciplinary tumor diagnostics. While the preprocessing pipeline was optimized for brain MRI, adaptation will be necessary for its application to other anatomical regions or tumor types. Another limitation is the interpretability of the models, which requires further improvement to enhance clinical trust and usability.

Future research will focus on overcoming these limitations by extending the framework to include 3D volumetric MRI and multi-modal MRI sequences such as T1, T2, FLAIR, and contrast-enhanced imaging, with larger and more diverse clinical datasets such as BraTS, ensuring greater robustness and generalization. Optimization of YOLO-v11 for deployment on low-power edge devices, such as embedded GPUs and Raspberry Pi, will enable real-time diagnostics at the point of care. In addition, enhancing model interpretability will be prioritized to support clinical decision-making and facilitate adoption in medical practice. Ultimately, this work aspires to deliver a comprehensive, real-time, and clinically viable deep learning framework for brain tumor detection and segmentation, significantly advancing the field of automated medical imaging diagnostics.

# DECLARATIONS

**Acknowledgement:** We appreciate the generous support from all the contributor of research

and their different affiliations.

**Funding:** No funding body in the public, private, or nonprofit sectors provided a particular grant for this research.

**Availability of data and material:** In the approach, the data sources for the variables are stated.

**Authors' contributions:** Each author participated equally to the creation of this work.

**Conflicts of Interests:** The authors declare no conflict of interest.

**Consent to Participate:** Yes

**Consent for publication and Ethical approval:** Because this study does not include human or animal data, ethical approval is not required for publication. All authors have given their consent.

# REFERENCES

Aftab, M., Mehmood, F., Sahibzada, K. I., Zhang, C., Jiang, Y., & Liu, K. (2025). Attention-Enhanced Multi-Task Deep Learning Model for Classification and Segmentation of Esophageal Lesions. *ACS Omega*. https://doi.org/10.1021/acsomega.4c10763

Aftab, M., Mehmood, F., Zhang, C., Nadeem, A., Dong, Z., Jiang, Y., & Liu, K. (2025). *AI in Oncology: Transforming Cancer Detection through Machine Learning and Deep Learning Applications*.

Alnageeb, M. H. O., & M.H., S. (2025). Real-time brain tumor diagnoses using a novel lightweight deep learning model. *Computers in Biology and Medicine*, *192*. https://doi.org/10.1016/j.compbiomed.2025.110242

AlShowarah, S. A. (2025). DeepCancer: deep learning for brain tumor detection-based application system. *Neural Computing and Applications*, *37*(7), 5577–5596. https://doi.org/10.1007/s00521-024-10926-4

Alsufyani, A. (2025). Performance comparison of deep learning models for MRI-based brain tumor detection. *AIMS Bioengineering*, *12*(1), 1–21. https://doi.org/10.3934/bioeng.2025001

Bai, R. (2025). *SCC-YOLO: An Improved Object Detector for Assisting in Brain Tumor Diagnosis*.

Baid, U., Ghodasara, S., Mohan, S., Bilello, M., Calabrese, E., Colak, E., Farahani, K., Kalpathy-Cramer, J., Kitamura, F. C., Pati, S., Prevedello, L. M., Rudie, J. D., Sako, C., Shinohara, R. T., Bergquist, T., Chai, R., Eddy, J., Elliott, J., Reade, W., … Bakas, S. (2021). *The RSNA-ASNR-MICCAI BraTS 2021 Benchmark on Brain Tumor Segmentation and Radiogenomic Classification*.

Batool, A., & Byun, Y. C. (2025). A lightweight multi-path convolutional neural network architecture using optimal feature selection for multiclass classification of brain tumors using magnetic resonance images. *Results in Engineering*, *25*. https://doi.org/10.1016/j.rineng.2025.104327

Bin Shabbir Mugdha, S., & Uddin, M. (2025). NeuroSight: A Deep-Learning Integrated Efficient Approach to Brain Tumor Detection. *Engineering Reports*, *7*(1). https://doi.org/10.1002/eng2.13100

Deng, K., Wen, Q., Yang, F., Ouyang, H., Shi, Z., Shuai, S., & Wu, Z. (2025). OS-DETR: End-to-end brain tumor detection framework based on orthogonal channel shuffle networks. *PLoS ONE*, *20*. https://doi.org/10.1371/journal.pone.0320757

Dulal, R., & Dulal, R. (2025). *Brain Tumor Identification using Improved YOLOv8*.

*Enhanced MRI-Based Brain Tumor Detection and Classification Using YOLO-v11*. (n.d.). Https://Www.Researchgate.Net/Publication/391495593_Enhanced_MRI-Based_Brain_Tumor_Detection_and_Classification_Using_YOLO-v11.

Golkarieh, A., Rezvani Boroujeni, S., Kiashemshaki, K., Deldadehasl, M., Aghayarzadeh, H., & Ramezani, A. (2025). Breakthroughs in Brain Tumor Detection: Leveraging Deep Learning and Transfer Learning for MRI-Based Classification. *Computer and Decision Making: An International Journal*, *2*, 708–722. https://doi.org/10.59543/comdem.v2i.14243

Hezil, N., Benzaoui, A., Souami, F., Bentrcia, Y., Amrouche, A., Belattar, K., & Bouridane, A. (2025). Deep learning-based robust brain tumor detection via fuzzy C-means and LSTM

networks. *Network Modeling Analysis in Health Informatics and Bioinformatics*, *14*(1). https://doi.org/10.1007/s13721-025-00504-6

Hosny, K. M., Mohammed, M. A., Salama, R. A., & Elshewey, A. M. (2025). Explainable ensemble deep learning-based model for brain tumor detection and classification. *Neural Computing and Applications*, *37*(3), 1289–1306. https://doi.org/10.1007/s00521-024-10401-0

K, S. K., A. R. K., P H., & N S. (2025). Automated Brain Tumor Detection And Localization Using YOLO-Based Deep Learning Algorithm. *American Journal of Psychiatric Rehabilitation*, *28*. https://doi.org/10.69980/ajpr.v28i5.356

Kang, M., Ting, F. F., Phan, R. C. W., & Ting, C. M. (2025). PK-YOLO: Pretrained Knowledge Guided YOLO for Brain Tumor Detection in Multiplanar MRI Slices. *Proceedings - 2025 IEEE Winter Conference on Applications of Computer Vision, WACV 2025*, 3732–3741. https://doi.org/10.1109/WACV61041.2025.00367

M, M. M., T. R, M., V, V. K., & Guluwadi, S. (2024). Enhancing brain tumor detection in MRI images through explainable AI using Grad-CAM with ResNet 50. *BMC Medical Imaging*, *24*. https://doi.org/10.1186/s12880-024-01292-7

Mathivanan, S. K., Srinivasan, S., Koti, M. S., Kushwah, V. S., Joseph, R. B., & Shah, M. A. (2025). A secure hybrid deep learning framework for brain tumor detection and classification. *Journal of Big Data*, *12*(1). https://doi.org/10.1186/s40537-025-01117-6

Mijwil, M. M. (2024). Smart architectures: computerized classification of brain tumors from MRI images utilizing deep learning approaches. *Multimedia Tools and Applications*. https://doi.org/10.1007/s11042-024-20349-x

Monisha, S. M. A., & Rahman, R. (2025). *Brain Tumor Detection in MRI Based on Federated Learning with YOLO-v11*.

Muksimova, S., Umirzakova, S., Mardieva, S., Iskhakova, N., Sultanov, M., & Cho, Y. I. (2025). A lightweight attention-driven YOLOv5m model for improved brain tumor detection. *Computers in Biology and Medicine*, *188*. https://doi.org/10.1016/j.compbiomed.2025.109893

Nadeem, M. Bin, Ali, A., Aziz, M. W., Ghani, M. U., Mustafa, G., & Farooq, A. B. (2024). *Automated Brain Tumor Detection via Transfer Learning Techniques*. Https://Www.Jcbi.Org/Index.Php/Main/Article/View/477.

Nahiduzzaman, M., Abdulrazak, L. F., Kibria, H. B., Khandakar, A., Ayari, M. A., Ahamed, M. F., Ahsan, M., Haider, J., Moni, M. A., & Kowalski, M. (2025). A hybrid explainable model based on advanced machine learning and deep learning models for classifying brain tumors using MRI images. *Scientific Reports*, *15*(1). https://doi.org/10.1038/s41598-025-85874-7

Onaizah, A. N., Xia, Y., & Hussain, K. (2025). FL-SiCNN: An improved brain tumor diagnosis using a siamese convolutional neural network in a peer-to-peer federated learning approach. *Alexandria Engineering Journal*, *114*, 1–11. https://doi.org/10.1016/j.aej.2024.11.063

Pande, Y., & Chaki, J. (2025). Brain tumor detection across diverse MR images: An automated triple-module approach integrating reduced fused deep features and machine learning. *Results in Engineering*, *25*. https://doi.org/10.1016/j.rineng.2024.103832

Pasunoori, K. C., Rajendra Prasad, C., & Raj Kumar, K. (2025). Deep Learning based Brain Tumor Detection using YOLO11n and Segmentation using SAM2 Model. *3rd International Conference on Intelligent Data Communication Technologies and Internet of Things, IDCIoT 2025*, 1414–1418. https://doi.org/10.1109/IDCIOT64235.2025.10914773

Rasool, N., Wani, N. A., Bhat, J. I., Saharan, S., Sharma, V. K., Alsulami, B. S., Alsharif, H., & Lytras, M. D. (2025). CNN-TumorNet: leveraging explainability in deep learning for precise brain tumor diagnosis on MRI images. *Frontiers in Oncology*, *15*. https://doi.org/10.3389/fonc.2025.1554559

Rastogi, D., Johri, P., Donelli, M., Kumar, L., Bindewari, S., Raghav, A., & Khatri, S. K. (2025a). Brain Tumor Detection and Prediction in MRI Images Utilizing a Fine-Tuned Transfer Learning Model Integrated Within Deep Learning Frameworks. *Life*, *15*. https://doi.org/10.3390/life15030327

Rastogi, D., Johri, P., Donelli, M., Kumar, L., Bindewari, S., Raghav, A., & Khatri, S. K. (2025b). Brain Tumor Detection and Prediction in MRI Images Utilizing a Fine-Tuned Transfer Learning Model Integrated Within Deep Learning Frameworks. Life, 15(3). https://doi.org/10.3390/life15030327

Rivera, E. F., Falconí, D. Q., & Calero, H. O. (2025). *Application of YOLO Models for Assisted Tumor Diagnosis: A Computer Vision-Based Approach*. https://doi.org/10.20944/preprints202502.1402.v1

Sajid, S., Hussain, S., & Sarwar, A. (2019). Brain Tumor Detection and Segmentation in MR Images Using Deep Learning. *Arabian Journal for Science and Engineering*, *44*(11), 9249–9261. https://doi.org/10.1007/S13369-019-03967-8/METRICS

Shoaib, M. R., Zhao, J., Emara, H. M., Mubarak, A. S., Omer, O. A., Abd El-Samie, F. E., & Esmaiel, H. (2025). Improving brain tumor classification: Integrating pre-trained CNN models and machine learning algorithms. *Heliyon*, *11*(10). https://doi.org/10.1016/j.heliyon.2024.e33471

Siegel, R. L., Miller, K. D., Wagle, N. S., & Jemal, A. (2023). Cancer statistics, 2023. *CA: A Cancer Journal for Clinicians*, *73*, 17–48. https://doi.org/10.3322/caac.21763

Sokea, C., & Marina, S. (2025). Improving Diagnostic Accuracy of Brain Tumor MRI Classification Using Generative AI and Deep Learning Techniques. *Babylonian Journal of Artificial Intelligence*, *2025*, 55–63. https://doi.org/10.58496/bjai/2025/005

Taha, A. M., Aly, S. A., & Darwish, M. F. (2025). *Detecting Glioma, Meningioma, Pituitary Tumors, and Normal Brain Tissues based on YOLO-v11 and YOLOv8 Deep Learning Models*.

Wahidin, M. F., & Kosala, G. (2025). Brain Tumor Detection Using YOLO Models in MRI Images. *ICADEIS 2025 - 2025 International Conference on Advancement in Data Science, E-Learning and Information System: Integrating Data Science and Information System, Proceedings*. https://doi.org/10.1109/ICADEIS65852.2025.10933433

Wekalao, J., Ali, Y. A. A., Saidani, T., Patel, S. K., Almawgani, A. H. M., & Alabsi, B. A. (2025). A Graphene-Based Surface Plasmon Resonance Metasurfaces Terahertz Sensor for Early Brain Tumor Detection with Machine Learning Optimization. *Plasmonics*. https://doi.org/10.1007/s11468-025-02930-8

Yang, T., Lu, X., Yang, L., Yang, M., Chen, J., & Zhao, H. (2024). Application of an MRI image segmentation algorithm for brain tumors based on improved YOLO. *Frontiers in Neuroscience*, *18*. https://doi.org/10.3389/fnins.2024.1510175

Zafar, W., Husnain, G., Iqbal, A., Alzahrani, A. S., Irfan, M. A., Ghadi, Y. Y., Al-Zahrani, M. S., & Naidu, R. S. (2024). Enhanced TumorNet: Leveraging YOLOv8s and U-net for superior brain tumor detection and segmentation utilizing MRI scans. *Results in Engineering*, *24*. https://doi.org/10.1016/j.rineng.2024.102994

Zulfqar, S., Zia, M. A., Mehmood, F., Pervez, A., & Abbas, T. (2024). *Breast Cancer Diagnosis: A Transfer Learning-based System for Detection of Invasive Ductal Carcinoma (IDC)*. Https://Jcbi.Org/Index.Php/Main/Article/View/394.